Terahertz Imaging Systems With Aperture Synthesis Techniques

Viktor Krozer, *Senior Member, IEEE*, Torsten Löffler, Jørgen Dall, *Member, IEEE*, Anders Kusk, *Member, IEEE*, Finn Eichhorn, Rasmus Kjelsmark Olsson, Jonas Due Buron, Peter Uhd Jepsen, Vitaliy Zhurbenko, *Member, IEEE*, and Thomas Jensen

***Abstract*—This paper presents the research and development of two terahertz imaging systems based on photonic and electronic principles, respectively. As part of this study, a survey of ongoing research in the field of terahertz imaging is provided focusing on security applications. Existing terahertz imaging systems are reviewed in terms of the employed architecture and data processing strategies. Active multichannel measurement method is found to be promising for real-time applications among the various terahertz imaging techniques and is chosen as a basis for the imaging instruments presented in this paper. An active system operation allows for a wide dynamic range, which is important for image quality. The described instruments employ a multichannel high-sensitivity heterodyne architecture and aperture filling techniques, with close to real-time image acquisition time. In the case of the photonic imaging system, mechanical scanning is completely obsolete. We show 2-D images of simulated 3-D image data for both systems. The reconstruction algorithms are suitable for 3-D real-time operation, only limited by mechanical scanning.**

***Index Terms*—Femtosecond systems, photonic detectors, photonic systems, submillimeter-wave imaging, submillimeter-wave technology, synthetic aperture imaging, synthetic aperture radar, terahertz imaging.**

I. Introduction

THE MAJOR driving force for development of terahertz imaging systems today originates from security applications and, in particular, stand-off imaging of persons and hidden objects for security enforcement, including illicit drug and explosives detection. Bonding flaw and defect detection at stand-off distances for space applications requires imaging systems with similar performance as those for security applications. Hence, system concepts can be discussed jointly for both applications. By terahertz, we mean a frequency range covering 300–3000 GHz, the lower part of which (100–1000 GHz) is sometimes referred to as the submillimeter-wave frequency region.

Conventional imaging systems utilize optical and X-ray imaging for stand-off detection for security and space applications [1]–[3], although a number of millimeter-wave, submillimeter-wave, and terahertz imaging systems have been presented [4]–[18]. In general, discussion on imaging systems can be broken down into passive imaging systems utilizing natural radiation or reflection and active imaging systems employing a dedicated source or an array of sources. Several recent overviews have been published on this subject [12], [16], [17], [19]–[21]. Another distinction on system level is time-domain versus frequency-domain operation.

This paper has two goals. The first one is to review imaging systems and algorithms at millimeter-wave and terahertz frequencies, subsequently called terahertz cameras. The second goal is to present two new imaging systems being developed by the authors.

The review focuses on active systems geared towards stand-off detection and fast image processing for nondestructive testing and security applications. Active imaging systems are preferred in unfavorable environmental conditions [19]. The resolution and the scene size require either an array or a scanning imaging architecture [22], [23]. Small receiver arrays have recently been presented in [24] and [25].

We will review systems based on electronic and photonic principles and provide a short description of imaging techniques and algorithms reported in the literature. As to electronic imaging systems, we mean those systems relying entirely on electronic components, whereas photonic imaging systems are those where a terahertz signal is generated or received through transformation of an optical signal into the terahertz range. Applications demanding spectroscopic capabilities for biological and chemical substance recognition are feasible at frequencies beyond 500 GHz, which are realized in this paper using a femtosecond multichannel imaging system.

One scenario considered in this paper is illustrated schematically in Fig. 1 and consists of an active array of transmitters and receivers illuminating an object at stand-off distance. The receivers are place in the center part of the array, while the transmitters are situated at larger distances. The major imaging task here is to detect an object at a distance and classify the object

Manuscript received December 01, 2009; revised May 03, 2010; accepted May 03, 2010. Date of publication June 28, 2010; date of current version July 14, 2010. This work was supported in part by the European Space and Technology Center, European Space Agency, under Contract 21155/07/NL/ST. The work of F. Eichhorn and R. K. Olsson was supported by the Photonics Academy Denmark and NKT Photonics A/S.

V. Krozer was with the Electromagnetic Systems, DTU Elektro, Technical University of Denmark, DK-2100 Copenhagen, Denmark. He is now with the Physics Department, Johann Wolfgang Goethe University of Frankfurt, 60438 Frankfurt, Germany (e-mail: Krozer@physik.uni-frankfurt.de).

T. Löffler is with SynView GmbH, 61479 Frankfurt, Germany (e-mail: TL@synview.com).

J. Dall and A. Kusk are with DTU Space, Technical University of Denmark, DK-2100 Copenhagen, Denmark (e-mail: jd@space.dtu.dk).

F. Eichhorn, R. K. Olsson, J. D. Buron, and P. U. Jepsen are with Terahertz Technologies and Biophotonics, DTU Fotonik, Technical University of Denmark, DK-2100 Copenhagen, Denmark (e-mail: puje@fotonik.dtu.dk).

V. Zhurbenko and T. Jensen are with Electromagnetic Systems, DTU Elektro, Technical University of Denmark, DK-2100 Copenhagen, Denmark (e-mail: vk@elektro.dtu.dk).

Color versions of one or more of the figures in this paper are available online at http://ieeexplore.ieee.org.

Digital Object Identifier 10.1109/TMTT.2010.2050246

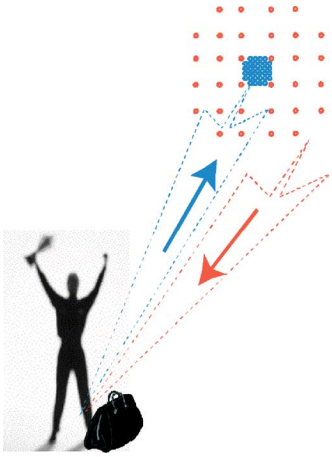

Fig. 1. Typical imaging scenario for stand-off detection using an active array of 32 transmitters (red, online version) and 32 receivers (blue, online version).

with regards to its potential threat or impact. One would like to detect all possible materials (i.e., solid, fluid, or gaseous) with many different properties (e.g., metal or dielectric). An imaging system in such a scenario should be able to detect the object with high spatial resolution and should classify this object with high success rate or low false alarm rate. The imaging should be close to real time in security applications with somewhat relaxed demands for industrial applications.

The terahertz camera considered here should operate at stand-off distances of a few meters to tens of meters, image man-sized scenes and produce images close to real time, and detect objects with a minimum size of a few centimeters. The bandwidth of the terahertz camera should therefore be large for good range resolution.

In the case of terahertz imaging systems based on photonic continuous-wave (CW) or pulsed techniques, the power is not sufficient to operate at such large distances, but the resolution is much better. This is due to the high operating frequencies. In this case, it is advantageous to operate a photonic terahertz imaging system at a closer distance in order to obtain submillimeter range and cross-range resolution. In fact, with the bandwidth of such systems, the range resolution is in the range of tens of micrometers.

II. Survey of Electronic Imaging Systems

Active systems can operate in monostatic, bi-static, or multistatic mode. An advantage of active systems is the possibility for bi-static or multistatic measurements, providing information on the reflection and transmission properties of the object, which can be fully exploited in image processing algorithms. Passive systems operate only in an observation mode or with a broadband incoherent source, which then acts as a signal source [26]. However, powerful broadband noise sources are very difficult to realize. In principle, both passive and active imaging systems are feasible for the applications considered. Heterodyne millimeter-wave systems at room temperature require local oscillator (LO) signal sources, which can be used for object illumination.

Experiments demonstrated in literature [27]–[32] show that millimeter-wave frequencies ($<$ 100–300 GHz) are sufficient for good detection with high resolution while offering less complex systems and exhibiting better signal-to-noise ratios (SNRs) as compared with systems operating at higher frequencies. Another advantage of imaging systems at millimeter waves, as compared with terahertz systems, is the availability of integrated components and, in the near future, active monolithic integrated front-end modules, which would make multielement systems economically feasible. On the other hand, current experimental results reveal limited spectral features for substances such as explosives below 500 GHz and slightly lower frequencies for other materials [12].

A. Passive Imaging Techniques

A passive imaging system is essentially a radiometer, which detects the radiation emitted from an object in view. One can employ either direct-detection focal plane arrays [33], [34] or a heterodyne receiver with a scanning system and single element receiver [35]–[40]. Passive multichip millimeter-wave imaging systems have been demonstrated in [41]–[46]. Direct-detection receivers have been using millimeter-wave monolithic microwave integrated circuit (MMIC) technology [10], [47] with good noise performance [4], [5], [8], [48]–[50], however, without dual-polarization and phase-detection capabilities. However, interferometric imaging requires the determination of the amplitude and phase of the detected signal [51], [52]. For adequate spatial resolution at large stand-off distances, apertures need to be large, i.e., of the order of 1-m diameter, and scanning should be employed [39], [53]–[55]. Other low-scan-rate mechanical systems have been developed in [56]–[58], and an alternative technology using a microbolometer cryogenic millimeter-wave focal plane array has been pursued in [33] and [58]. A stereoscopic passive imaging system has been presented in [59]. Recently, focal plane arrays at submillimeter-wave frequencies have been demonstrated operating at room temperature and using a standard CMOS process [14], [60], [61].

It is anticipated that, in the near future, MMIC technology will become the technology of choice from a cost and performance point of view, providing a natural path towards multichannel imaging systems.

B. Active Imaging Techniques

Active imaging systems employ a transmitter to illuminate the scene and a receiver to collect the scattered energy, or multiples of either transmitters (Tx) or receivers (Rx), or both. Active imaging systems operating over a wide frequency range have been presented for security [3]–[18], [62]–[64] and biological [65], [66] applications.

In the case of arrays, one can imagine either focal plane or interferometric arrays including aperture filling techniques described below. Also, the receiver channels can use bolometric detection (direct detection) schemes or heterodyne receiver architectures. The latter is preferred in the case of active imaging systems due to the improved sensitivity, which could be two to three orders of magnitude better as compared with direct detection and provide micrometer-range resolution with large-bandwidth systems and utilizing the phase information.

Active imaging systems have the fundamental benefit of being independent of natural emission of the object and can therefore be successfully employed indoors and outdoors for concealed objects, even with thick cover materials, and are only limited by the available transmit power and receiver sensitivity. Another very important benefit is that the IF frequency bandwidth does not determine the overall system performance. Hence, IF frequency can be chosen as low as a few megahertz.

It should be emphasized that the emitted power is of the order of $<$ 10 mW and still well below any known health hazards [67] and therefore regarded as completely harmless. Thus, this technique could be ideal for large view scanning of populated areas.

A fully focused diffraction-limited 3-D image of a person or imaged target has been presented in [68] by scanning an inward-directed vertical array around the person or imaged target. The array achieved a full 360° mechanical scan in 2–10 s with optimized illumination, which minimizes signal loss due to specular reflection away from the array.

Time-domain electronic imaging systems utilize a pulse generated by fast switching of diodes [69], [70] or transistors [71] with bandwidths approaching those of photonic systems. In this case, all energy is concentrated in the pulse itself, which then should exhibit a sufficient energy level at all frequencies. Terahertz time-domain systems utilizing windowed Fourier transformation in 3-D have been presented in [72] and [73], and wide-angle tomographic imaging in synthetic aperture radar (SAR) has been reported in [74] employing mappings to modify the convolution-back projection method of computed tomography. Reconstructions from circular-arc projections that are made using the algorithm are of the same high quality as those made from standard straight-line projections.

C. Scanners

A number of mechanically scanned optical systems have been developed, such as the spherical scanning antenna, the Lewis scanner, the Schwarzschild scanner, and the Rotman lens scanner [75]. Also, there is the scanning spherical trireflector antenna [76], the two-mirror scanning system [77], and the millimeter-wave monopulse twist reflector scanning antenna [78]. The oscillating motion of the mirrors used in these later designs is too slow to produce real-time scanning. A rotating polygon scanner [79], however, can scan at rates up to 50 kHz with scan angles approaching 180°. A high-speed scanning mirror [80] has formed the basis for a millimeter-wave line-scan system for use in airborne applications. Other imagers [81] achieve a raster scan by motion of both the antenna and receivers.

None of the systems described above are considered adequate for low-cost real-time imaging systems. Most commercial imaging systems employ some kind of scanners, with the exception of a recent electronically scanning system presented in [55] and [82].

It is therefore suggested not to use a scanner if a number of $>$16 Tx and Rx channels can be afforded. Alternatively, one can use a linear array of elements for the imaging system and employ a simple scanner using a plane rotating mirror. This has the advantage that optical defocusing and aberrations are kept to a minimum.

III. Survey of Photonic Imaging Systems

Photonic terahertz imaging systems have predominantly been employing time-of-flight measurements by raster scanning the imaging object. Recently, more advanced proposals for terahertz synthetic aperture and interferometric imaging methods have been proposed by several groups and published both in the scientific literature and filed as patents. A comprehensive review of imaging with terahertz radiation has recently been published in [11], [12], and [85]–[88].

In practice, until today, most systems employ one Tx/Rx pair by moving the transmitter and/or receiver around the imaging object, acquiring data from various positions and subsequently reconstructing an image. Having more than one transmitter and/or receiver at different positions enables illumination of an object from more than one location and, hence, employs tomography. The advent of the fiber-coupled photoconductive emitters/receivers made this a viable method [89]–[92]. Below, we will demonstrate a possible implementation of a multichannel imaging system using fiber-coupled sensor heads.

Several research groups have explored the analogy of X-ray computer tomography (CT) with terahertz radiation and pioneered by Zhang *et al.* [91]. In contrast to X-ray CT, terahertz CT resolves both the amplitude and the phase information of the scattering object. As a consequence, the terahertz CT image contains more information than the X-ray CT about the target, such as the frequency-resolved refractive index. The wide-aperture reflection tomography allows tomographic reconstruction of a series of slices measured at different view angles [94]. This technique works best with strong reflectors such as metals. The algorithms used for the reconstruction of the images are in general filtered back-projection algorithms.

IV. Survey of Imaging Algorithms for Terahertz and Millimeter-Wave Systems

Focusing the raw terahertz data of a terahertz imaging system for security and space applications is a challenging task due to the required real-time processing, 3-D mapping, the comparable object and antenna aperture size with the stand-off distance, the relatively large bandwidth reaching 1000 GHz, and the adoption of the bi-static configuration [95].

One review [96] covers the fundamental principles of radar imaging addressing aspects of through-wall radar imaging, radar detection of buried targets, tomography and detection of concealed weapons, and passive bi-static radar.

A. Resolution

The theoretical range resolution ρ depends on the bandwidth of the transmitted signal B [98]

$$\rho = \frac{c}{2B}. \tag{1}$$

A 2-cm resolution, for instance, requires a 7.5-GHz bandwidth without additional phase processing.

In the cross-range direction, a passive diffraction-limited system would offer an angular resolution of

$$\alpha = \frac{\lambda}{D} \tag{2}$$

where λ is the wavelength of the incident radiation and D is the diameter of the aperture. The spatial cross-range resolution is found by multiplying α (in radians) with the range to the object. For an active monostatic system, the angular resolution is half of that in (2) [98], whereas, for a multistatic system like that in Fig. 1, (2) holds true for an object in the far field, as the effective size of the aperture is half the size of the transmitter aperture D.

A multistatic radar transmits sequentially on each of the N_{TX} TX antennas and receives the scattered signal simultaneously on each of the N_{RX} RX antennas. For a TX, RX element pair, the round-trip equirange surfaces are ellipsoids, which in the far field approximate spheres centered at the midpoint between the TX and RX antennas.

The angular field of view (FOV) is determined by the smaller of two angles: the antenna element beam width and the angular ambiguity spacing (grating lobe spacing). If the beam width exceeds the ambiguity spacing, the imaged object must be sufficiently small to fit in between two ambiguities.

The angular ambiguity spacing θ depends on the effective element spacing d

$$\theta = \frac{\lambda}{d} = \frac{\lambda N}{D} \tag{3}$$

where N is the effective number of elements. Hence, large objects call for closely spaced elements. Equation (3) applies to a multistatic system, for which the ambiguity spacing is twice that of a monostatic radar system [99], as its effective elements spacing is half of the physical element spacing.

The maximum number of cross-range pixels that can be resolved N_{cr} is the ratio of the ambiguity spacing to the angular resolution

$$N_{\mathrm{cr}} = \frac{\theta}{\alpha} \tag{4}$$

which, according to (2) and (3), equals the effective number of array elements N. As an example, an imager with a 1-m aperture operating at a wavelength of 1 mm and covering a FOV of 12° would have an angular resolution of 0.06°, and it would call for at least 200 elements and produce the same number of uncorrelated pixels. For comparison, a typical thermal imager operating at 10 μm and having an objective diameter of 50 mm and an FOV of 12° has a theoretical number of pixels of about 1000. In practice, aberrations introduced by the detector array lower this value to be closer to 500.

B. Aperture Filling

In order to avoid grating lobes while obtaining the best possible resolution and the maximum unambiguous scene size with a given number of antenna elements, the $N_{\mathrm{TX}}N_{\mathrm{RX}}$ midpoints must be equidistantly spaced. This can be obtained with a TX antenna element spacing of

$$\Delta_{\mathrm{TX}} = N_{\mathrm{RX}}\Delta_{\mathrm{RX}} \tag{5}$$

where Δ_{RX} is the RX antenna element spacing. (Here and in the following, the TX elements are the more widely spaced elements, but TX and RX can obviously be interchanged.) It is noted that (5) implies no redundancy in the sense that no TX–RX midpoints coincide. The overall size of the antenna array is $N_{\mathrm{TX}}\Delta_{\mathrm{TX}} = N_{\mathrm{TX}}N_{RX}\Delta_{\mathrm{RX}}$, which offers an angular resolution of

$$\alpha = \frac{\lambda}{N_{\mathrm{TX}}N_{\mathrm{RX}}\Delta_{\mathrm{RX}}}. \tag{6}$$

The angular ambiguity separation is

$$\theta = \frac{\lambda}{\Delta_{\mathrm{RX}}} = N_{\mathrm{TX}}N_{\mathrm{RX}}\alpha. \tag{7}$$

Hence, a multistatic radar with $N_{\mathrm{TX}}+N_{\mathrm{RX}}$ antenna elements can resolve $N_{\mathrm{TX}}N_{\mathrm{RX}}$ uncorrelated pixels, which is typically much more than the $N_{\mathrm{TX}} + N_{\mathrm{RX}}$ pixels that can be resolved with a monostatic radar with the same number of elements. The same principle can be applied to a 2-D array [120].

It should be noted that the aperture filling outlined above is fundamentally different from that of synthetic aperture radiometers as used in radio astronomy [122] and in Earth observation [123]. Such correlation radiometers accomplish the aperture filling by cross correlating the signals received by any two pair of receiving elements. In order to fill the aperture, all multiples of the minimum baseline (i.e., the minimum element spacing) must be represented. Low-redundancy configurations are known for 1-D arrays, e.g., [99], but not for 2-D arrays [122]. For instance, the Y-shaped array adopted by the SMOS system does imply some redundancy.

Aperture filling by means of cross correlation cannot be applied to radar imaging of distributed targets because of the nonzero cross correlation of the signals scattered by different scatterers. However, for imaging of objects consisting of a few reflectors on a nonreflecting background, the principle may be applicable.

C. Range Focusing

A large time-bandwidth product of the transmitted signal is necessary in order to obtain a good SNR (long pulse) simultaneously with good resolution (large bandwidth). Using a delayed replica of the transmitted signal for demodulation, a target at a given range will result in a CW signal with a frequency proportional to the range from some reference range in deramp systems employing linear frequency-modulated (FM) signals. Hence, the focused range response can be obtained using a fast Fourier transform (FFT). The offset of the reference signal can be chosen so that a target at the range window center will exhibit a frequency of 0 Hz (with I/Q demodulation) or some IF frequency sufficiently low to allow digitization. For a scene with a range extent of Δr, the required IF bandwidth B_{IF} (and analog-to-digital converter (ADC) bandwidth) after analog deramp is a fraction of the modulation bandwidth B_p

$$B_{\mathrm{IF}} = \frac{2\Delta r}{c\tau_p}B_p = \frac{\tau_f}{\tau_p}B_p \qquad \text{(Deramp, single transmitter)}. \tag{8}$$

This simplifies the baseband system when the temporal range window τ_f is shorter than the uncompressed pulse length τ_p.

The minimum pulse length that must be recorded to focus the range window is $\tau_r = \tau_p + \tau_f$. For a system with multiple transmitters, it is desirable to transmit simultaneously on all transmitters in the array, separating the transmitted signals in frequency. The frequency separation Δf_{TX} should be small compared with the pulse bandwidth B_p (to allow SAR focusing as well as digitization) but larger than the B_{IF} given in (8) (to separate transmitters in the recorded data). The required IF and ADC bandwidth are then

$$B_{\mathrm{IF}} \geq N_{\mathrm{TX}} \Delta f_{\mathrm{TX}} \geq N_{\mathrm{TX}} \frac{\tau_f}{\tau_p} B_p \quad \text{(multiple transmitters)}. \tag{9}$$

The transmitters are easily separated after digitization, as the frequency offset is converted to a range offset by the range-focusing FFT. The ambiguous range is then determined by the transmitter frequency separation

$$r_{\mathrm{amb}} = \frac{c \Delta f_{\mathrm{TX}} \tau_p}{2 B_p}. \tag{10}$$

D. Cross-Range Focusing

The matched filter algorithm correlates raw data with the system point target response [97]. The shift-variance of the correlation step means that FFT-based filtering cannot be applied, resulting in a very large number of arithmetic operations per pixel. However, matched filtering is an optimum algorithm in that it does not exploit any approximations. Adjacent resolution-cell leakage (sidelobes) can be suppressed by amplitude weighting of the filter coefficients. Matched filtering is a very flexible algorithm, allowing for 2-D or 3-D focusing, without imposing any constraints on the placement of the antenna elements.

The mapping geometry of typical terahertz imaging systems is similar to that of spotlight SAR in the sense that a geometrically confined scene/object is illuminated by transmitter antenna elements having an angular separation with respect to the object. In its simplest, form, a spotlight SAR system is a monostatic radar with the object in the far field of the synthesized antenna. In this case, the simple rectangular algorithm [98] can be employed. Unfortunately, this is hardly applicable to terahertz imaging data, because the object is in the near field of the antenna array and a scatterer is not observed in the same range cell by all array elements. The Polar Format Algorithm [98]–[101] compensates to some extent for this phenomenon and can therefore be applied to scenes much larger than those covered by the rectangular format algorithm. Different formats have been studied in [102] including the close-range scenarios.

The SAR imaging process implies that the complex signals from all scatterers at the same round-trip range add up and form a sample of the (range-compressed) receive pulse. The result of the projection can be expressed as a sample of the Radon transform, which is the integral of the 3-D scene reflectivity over a plane [103]. The scene reflectivity can then be recovered by an inversion of the Radon transform for circular and spherical geometries [104] and for multistatic scenarios [105], [106]. A different approach has been proposed in [107], which utilizes the reversible transform between time delay and target boundary and has been applied to moving persons in [108], where moving motion of the persons was employed instead of scanning apertures.

One way of implementing the inverse Radon transform is the back projection algorithm (BPA), which is a spatial domain technique and, hence, somewhat computationally intensive. For every pulse and for every pixel in the output image, an interpolated sample must be computed and accumulated. "Fast" BPAs do exist [109]–[112], including near-field scenarios, with improvements in speed by a factor of 100 compared with direct back-projection in 2-D [111]. The advantage of these algorithms is that they provide some of the flexibility and robustness of a time-domain algorithm but exhibit a computational performance in parity with fast transform algorithms, e.g., the Fourier–Hankel or range migration algorithms (RMAs). Fast BPA for simple bi-static geometries have been proposed in [113] with a tradeoff in image quality. The BPA has also many attractive properties in common with the matched filtering: great flexibility, little constraint on the placement of the antenna elements, support of a large relative bandwidth, and a large relative aperture or object. It can be shown that with a perfect interpolator, the BPA is an exact inversion of the linear aperture SAR problem [111].

The RMA [114]–[116] is known under a number of different names, e.g., ω-k algorithm, wave equation technique, and seismic migration technique. For the center scatterer, the RMA is equivalent to the matched filter algorithm, and it is optimum in the same sense. However, the RMA implements the matched filtering in the spectral domain and, consequently, applies the same filter to the entire scene. For scatterers displaced from the scene center, a correction with the so-called Stolt transformation should be employed according to $K_Y = \sqrt{K_R^2 - K_X^2}$, which is a transformation from the range wavenumber in signal space K_R to the range wavenumber in object space K_Y. K_X is the cross-range wavenumber. The Stolt transformation corrects in a perfect way for the residual range migration and phase errors at all frequencies, but it is very sensitive to processing artifacts and offers little flexibility in the placement of the antenna elements. The RMA is well suited for wideband systems and for near-field systems with large apertures or large objects compared with the stand-off distance. A number of algorithms similar to RMA have been proposed, such as the chirp scaling algorithm [117], [118], where the final range inverse FFT is replaced by a single nonuniform FFT. Nonuniform FFT based projector/back projector with $O(N^2 \log(N))$ complexity has been presented in [119]. A comparison of the BPA and the RMA is provided in [121].

For real-time or close to real-time applications, it seems that the BPA is a good compromise between performance, flexibility, and speed.

V. Photonic Terahertz Multielement Imaging System Realization

As discussed above, most photonic imaging systems today utilize a single element with the mechanical according scanning, resulting in long acquisition times. The photonic terahertz imaging system presented here is based on an advanced dual-femtosecond fiber laser with an electronic delay stage unit, an all-fiber ultrashort pulse distribution system with dispersion

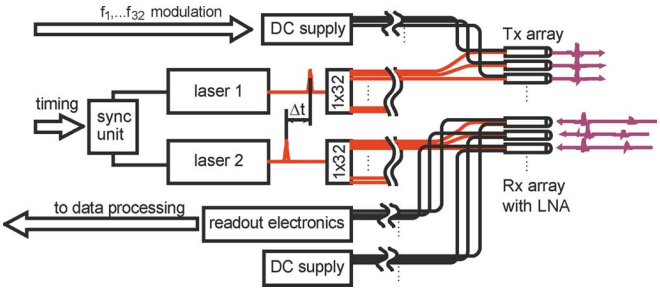

Fig. 2. Complete photonic terahertz imaging system, including electronic components. The thick arrows indicate communication with the data acquisition back-end.

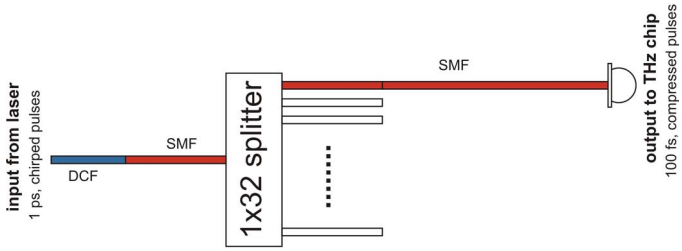

Fig. 3. Schematic of the fiber link. The input laser pulse is stretched in a 50-cm dispersion-compensating fiber (DCF) module with single-mode fiber (SMF) pigtails. The DCF module is spliced onto a 1×32 splitter, and each of these channels is spliced onto a piece of SMF (around 3 m) for pulse compression.

control [135], and a 2-D array of 32 individual terahertz emitters and 32 individual terahertz detectors. The advantage of an all-fiber design is a system that is very stable with respect to external vibrations and temperature fluctuations, without need for further alignment. In addition, we have developed ultra low-noise amplifiers, directly integrated into the individual terahertz receivers. Fig. 2 shows an outline of the principal components of the photonic imaging system. The first experimental results for this system are described below.

A. Laser System and Pulse Delivery

We have chosen a dual-femtosecond fiber-based laser system from Toptica Photonics AG with approximately 4.5 nJ per laser, 0.9-ps laser pulses around 1550 nm with a 90-MHz pulse repetition rate. The two femtosecond lasers are locked to the same repetition rate by active control, and the relative time delay can be adjusted electronically between 0.0–1.0 ns. This enables electronically controlled optical sampling (ECOPS). All laser pulses were measured by frequency-resolved optical gating (FROG) [134], and the retrieved pulses were compared with the measured intensity autocorrelation. The time jitter of the two synchronized lasers was characterized by measuring the intensity cross correlation.

It is a nontrivial task to distribute the high-power laser pulses to the 32-THz emitters and detectors. We have designed a fiber link, indicated in Fig. 3, in which the laser pulses are first stretched, then split into 32 channels, and finally compressed such that they are around 100 fs when they reach the emitters and detectors in order to obtain efficient terahertz generation. In this setup, the dominant nonlinear effect is self-phase modulation, which adds an intensity-dependent phase shift to the pulse. We first stretch the pulse for as large a fraction of the fiber link as possible using a dispersion-compensating fiber (DCF) module from OFS Fitel, resulting in a pulsewidth of around 2.2 ps. The stretched laser pulse is then split into 32 equal portions in a 1×32 power splitter from Ignis Photonyx capable of handling average optical powers < 440 mW. The insertion loss was around 1.5 dB. The normal dispersion of the DCF is compensated by the anomalous dispersion of the single-mode fiber (SMF) after the splitter. The optimal SMF fiber length of 4.6 m was found in a cut-back experiment, resulting in minimum pulse duration of 88 fs, as illustrated in Fig. 4.

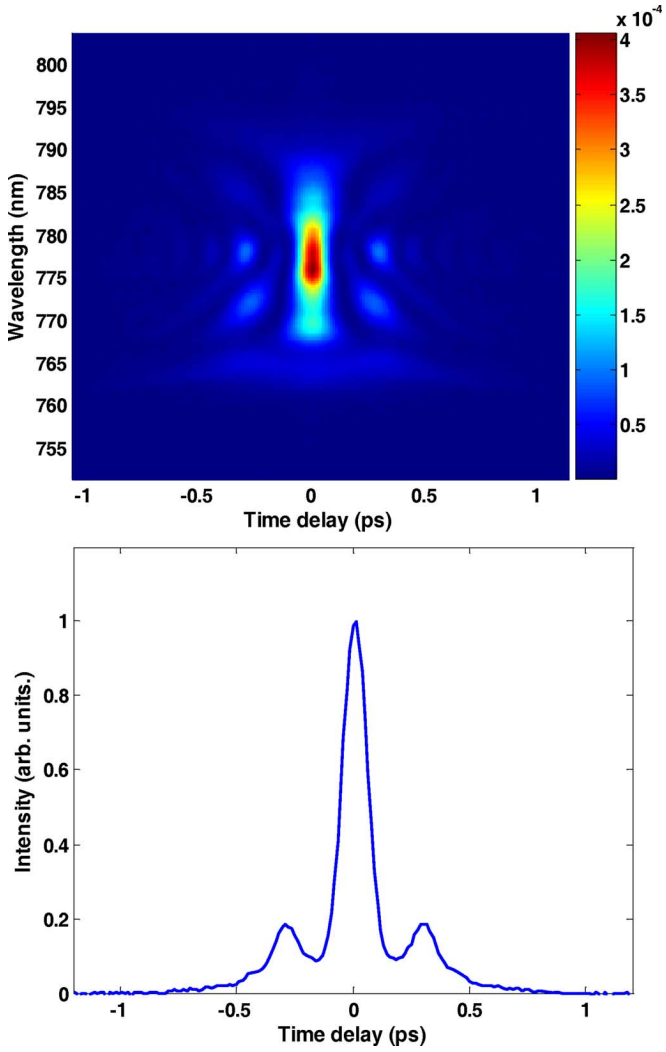

Fig. 4. Measurements of the laser pulse at the end of the fiber link. Top: Measured FROG trace. The FWHM of the retrieved pulse is 88 fs. Bottom: Intensity autocorrelation of the pulse. The FWHM of the autocorrelation is 131 fs.

B. Terahertz Emitters and Detectors

Both terahertz emitters and receivers use photoconductive switches to respectively generate and receive terahertz radiation [133] using low-temperature-grown InGaAs layers [91] at 1550 nm, which are commercially available from Menlo Systems GmbH.

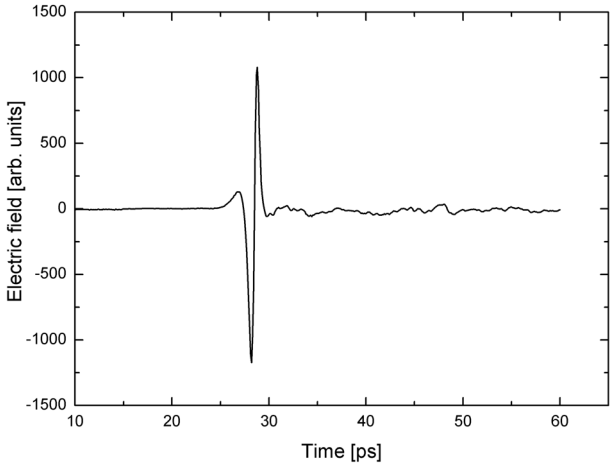

Fig. 5. Terahertz pulse generated and received with photoconductive switches from Menlo Systems fed by femtosecond laser pulses from the fiber link.

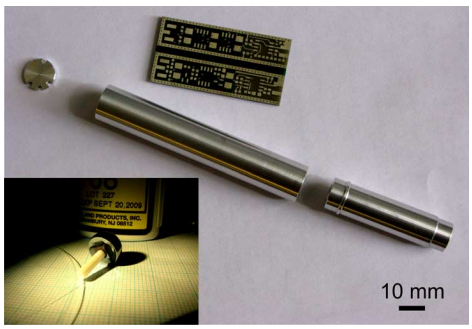

Fig. 6. Photograph of the parts of the terahertz sensor head. The diameter of the heads is 12 mm, and the total length is 130 mm. The silicon lenses have a diameter of 10 mm and are mounted into the rightmost part. The PCB shows the unpopulated current amplifier and fits into the tube shown in the center of the picture. Inset: The photoconductive antenna chip glued directly onto the silicon lens. The fiber link is butt-coupled into the photoconducting gap.

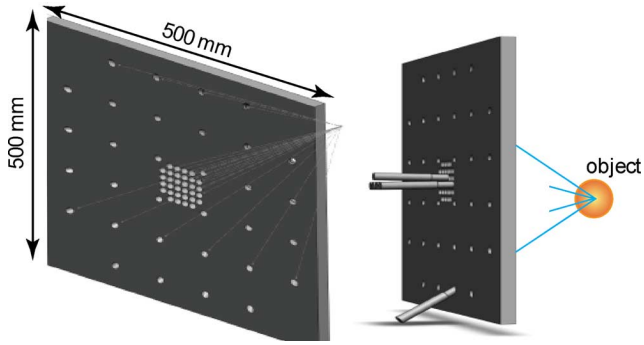

Fig. 7. 3-D rendering of the mounting structure for the photonic terahertz antenna array. Each element is directed towards the scene center by the structure. The receivers are placed in the inner array spaced by 13 mm and the transmitters in the outer array spaced by 80 mm.

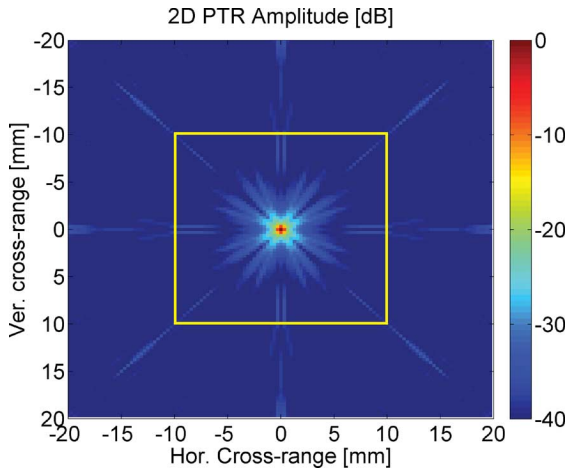

Fig. 8. Point target reconstruction simulation for the 32 × 32 element photonic array with a bandwidth of 100–1000 GHz. Red square (online version) indicates desired cross-range scene extent (2 cm × 2 cm).

The terahertz radiation is collimated out of the photoconductor using hyper-hemispherical high-resistivity silicon lenses. Fig. 5 shows a femtosecond terahertz pulse generated and received with the photoconductive switches described above and fed by direct butt-coupling of the fiber.

The ultracompact design of the transmitter and receiver head integrates silicon-lens, photoconductive switch, and, respectively, bias supply (in the emitter) and low-noise current amplifier (in the receiver) in one single compact unit, as depicted in Fig. 6. The custom-designed LNA preamplifier exhibits a transimpedance gain of 10^9 V/A, an equivalent noise voltage and current of $e_n \approx 6$ nV/sqrt(Hz), $i_n \approx 1$ fA/sqrt(Hz), with a bandwidth of ~ 20 kHz, and an input capacitance of ~ 3 pF.

C. Design of the 2-D Synthetic Aperture Array

The photonic system consists of a 2-D transmit/receive synthetic aperture array. The practical realization is depicted in Fig. 7. The 32 receivers are stacked in a 6×6 grid (corners omitted for ease of manufacturing) in the inner part of the array and spaced by 13 mm. The transmitter units are placed in the outer part and spaced by 80 mm. All units are fitted into a 20 mm × 500 mm × 500 mm aluminum mounting structure and pointing towards a center of scene at 300 mm from the structure.

The photonic terahertz imaging system has not yet been finalized, and therefore simulation results are shown in this paper to demonstrate the performance of the imaging system. All simulations were performed for a Gaussian pulse system with a bandwidth of 900 GHz centered around a frequency of 550 GHz. A simulated point target reconstruction is shown in Fig. 8, with the slice shown taken at the range of the point target. The simulated cross-range 3-dB resolution is 0.4 mm [consistent with (2)], and the first ambiguities are centered approximately 14 mm from the point target [consistent with (3)]. The ambiguities are smeared due to the large bandwidth employed and are 35 dB below the peak. If a full volume (2 cm (range) × 4 cm × 4 cm) is reconstructed and integrated in range, the peak relative ambiguity level rises to around −20 dB.

VI. Multielement Electronic Imaging System Realization

The electronic imaging system combines a horizontal, linear array of elements with vertically scanning optics and will be capable of scanning a 1 m × 2 m scene at a distance > 7-m scene

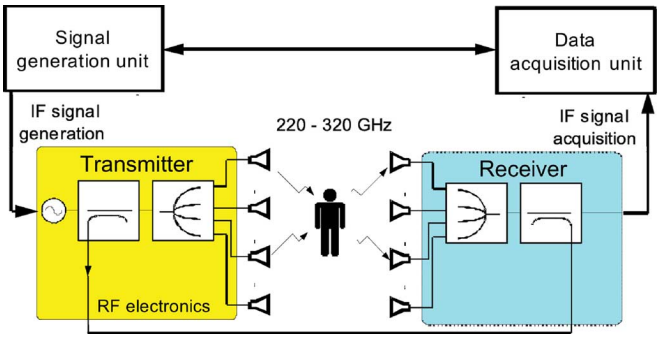

Fig. 9. Block diagram of the electronic imaging system. The component choice is given in the text.

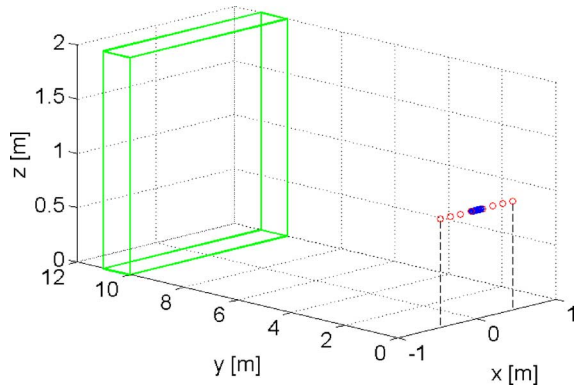

Fig. 10. Sketch of the scene (green, online version) and array configuration of the electronic imaging system with 16 receiving (blue, online version) and eight transmitting elements (red, online version) at a working distance of 10 m. The vertical scanning optics have been omitted for clarity.

with the according reflector dimensions. The image acquisition and processing is foreseen to be in real time, enabling imaging of moving objects. Using an image refresh rate of $t_{\mathrm{ref}} < 500$ ms and 100 lines in the vertical direction (2-cm resolution of a 2-m scene) leaves 5-ms/line acquisition time; this implies that the optical scanner has to move faster than this time. This puts high demands on the mechanical design and the data acquisition unit.

The suggested electronic imaging system features an array of Tx and Rx channels in multistatic configuration operating at 220–320 GHz (100-GHz bandwidth), a data acquisition and signal generation unit, as shown in Fig. 9. The delay line connecting the transmitter and the receiver is a fixed delay line employing a 50-Ω coaxial cable.

In general, front-end electronic components operate over a bandwidth typical for waveguide components. Wider bandwidth is currently very difficult to achieve in electronic systems [69]–[71], [84].

Wideband power dividers at the Ku-band have been developed to distribute the LO signals, which are then multiplied to the output frequency. The element spacing for the Tx and Rx units have been optimized for low redundancy in the array and large unambiguous scene, as discussed above. Currently, the system employs 16 Rx units and 8 Tx units with 8-mm receiver and 128-mm transmitter spacing at a stand off distance of 10 m, illustrated in Fig. 10.

One bottleneck in development of multichannel terahertz imaging systems is the data transfer of the acquired data.

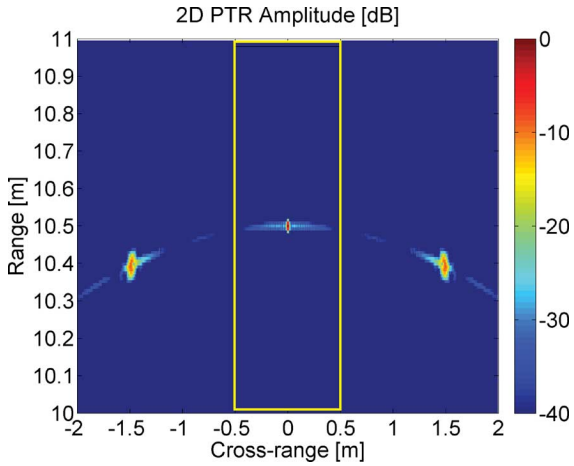

Fig. 11. Electronic imaging system simulated image reconstruction for a point target using the BPA. Red (online version) rectangle indicates desired scene size (1 m)—an extended scene was simulated to illustrate ambiguities.

For example, sampling the baseband image data from the imaging system with 30 MS/s in a 32-channel system with 2 bytes/sample and 10 images/s results in 1920-MB/s data stream, assuming an image acquisition time of 0.1 s/image. Such a huge data stream is difficult to support with standard commercial components utilizing, e.g., the PCIe bus. Also, the real-time computation of such large amounts of data is difficult to achieve using commercial off-the-shelf components. Using superheterodyne architectures alleviates this problem at the expense of larger complexity.

Synthetic aperture reconstruction for the configuration in Fig. 10 has been simulated assuming a point target at the center of the scene. The resulting x–y slice (z $=$ 1 m) is shown in Fig. 11. Hamming weighting of the aperture elements was employed to suppress cross-range sidelobes, giving a measured resolution of 1.4 cm, which is slightly larger than expected from (3), which does not assume weighting. Ambiguities are 1.5 m away from the point target, consistent with (4), and well outside the desired 1-m scene width. Real-time reconstruction was demonstrated using a parallel implementation of the BPA on an NVIDIA GTX260 graphics processing unit (GPU). A 1×1 m xy-slice of 128×128 pixels could be focused in less than 2 ms.

VII. Conclusion

This paper reviewed performance aspects of published terahertz imaging systems with special emphasis on security and object detection at stand-off distances. Literature results indicate that mechanical scanning represent a bottleneck in real-time imaging systems, whereas, for array imaging systems, one bottleneck is the data throughput. There is a clear tendency towards monolithic integration of front-ends for passive and active imaging systems. Imaging system parameters such as bandwidth, number of elements, element spacing, and antenna radiation pattern have been established for active electronic and photonic imaging systems, respectively. The discussion on most appropriate algorithms resulted in the choice of the BPA as the most suitable for real-time imaging system operation and good image quality.

Based on this discussion, an electronic and photonic terahertz imaging system has been demonstrated, and preliminary measured results for components of these systems have been shown. The overall system performance has been demonstrated using image reconstruction of point target data.

The photonic system comprises a fiber distribution system to the individual 32 Tx and 32 Rx units. Measured results indicate that 80-fs high-power pulses are obtained at the input to the respective terahertz antennas, which demonstrates state-of-the-art performance. Each terahertz antenna is integrated with state-of-the-art LNA. The Tx and Rx 2-D arrangement has been optimized for best image quality with a spatial resolution of 0.4 mm and an ambiguity level < -20 dB. The image processing speed for this imaging system is < 1 ms.

The electronic imaging system is based on a linear array operating in a frequency range of 220–320 GHz and employing an optical scanner for stand-off detection at > 7 m. It is demonstrated that the image processing for this system is < 2 ms with a spatial resolution of < 1.5 cm. The development of this system is still under way, but simulations of the overall system performance demonstrate that ambiguities are 1.5 m away from the point target, as necessary for person scanning. The reconstruction of the full scene of 1 m $\times$ 2 m is limited by the scanning mirror movement.

ACKNOWLEDGMENT

The authors would like to acknowledge the continuous support of Dr. P de Maagt and the European Space Agency. The authors would like to thank OFS Fitel Denmark ApS for supplying us with the DCF fiber modules. The authors would also like to acknowledge the anonymous reviewers for contributing to the improvement of this paper's final manuscript.

REFERENCES

[1] Wang and J. Li, "New requirement for cargo inspection system," *Port Technol. Int.* vol. PT18, p. 31/1, Spring 2003. [Online]. Available: http://www.porttechnology.org/

[2] J. Li and X. Wang, "Advanced X-ray container/vehicle inspection systems plus radiation detection subsystem: THSCAN™ fused technology," *Port Technol. Int.* vol. PT20, Autumn 2003. [Online]. Available: http://www.porttechnology.org/

[3] V. Krozer *et al.*, "KARIN: Key advanced research for identification and neutralisation terahertz camera for humanitarian demining and remote detection of chemical and biological substances, final Report," Eur. Space Agency, Noordwijk, The Netherlands, 2005, AO/1-4614/04/NL/LvH.

[4] D. M. Sheen, D. L. McMakin, T. E. Hall, and R. H. Severtsen, "Active millimeter-wave standoff and portal imaging techniques for personnel screening," in *Proc. IEEE Int. Conf. Technol. Homeland Security*, May 11–12, 2009, pp. 440–447.

[5] R. Appleby and H. B. Wallace, "Standoff detection of weapons and contraband in the 100 GHz to 1 THz region," *IEEE Trans. Antennas Propag.*, vol. 55, no. 11, pp. 2944–2956, Nov. 2007.

[6] M. C. Kemp, "Millimeter wave and terahertz technology for the detection of concealed threats – A review," in *Proc. IRMMW-THz Joint 32nd Int. Conf. Infrared Millim. Waves/15th Int. Conf. Terahertz Electron.*, Sep. 2–9, 2007, pp. 647–648.

[7] K. B. Cooper, R. J. Dengler, N. Llombart, T. Bryllert, G. Chattopadhyay, E. Schlecht, J. Gill, C. Lee, A. Skalare, I. Mehdi, and P. H. Siegel, "Penetrating 3-D imaging at 4- and 25-m range using a submillimeter-wave radar," *IEEE Trans. Microw. Theory Tech.*, vol. 56, no. 12, pp. 2771–2778, Dec. 2008.

[8] R. Appleby and R. N. Anderton, "Millimeter-wave and submillimeter-wave imaging for security and surveillance," *Proc. IEEE*, vol. 95, no. 8, pp. 1683–1690, Aug. 2007.

[9] R. J. Dengler, K. B. Cooper, N. Llombart, G. Chattopadhyay, T. Bryllert, I. Mehdi, and P. H. Siegel, "Toward real-time penetrating imaging radar at 670 GHz," in *IEEE MTT-S Int. Microw. Symp. Dig.*, 2009, pp. 941–944.

[10] I. Ederra, R. Gonzalo, B. E. J. Alderman, P. G. Huggard, B. P. de Hon, M. C. van Beurden, A. Murk, L. Marchand, and P. de Maagt, "Sub-millimeter-wave imaging array at 500 GHz based on 3-D electromagnetic-bandgap material," *IEEE Trans. Microw. Theory Tech.*, vol. 56, no. 11, pp. 2556–2565, Nov. 2008.

[11] W. Withayachumnankul, G. M. Png, X. Yin, S. Atakaramians, I. Jones, H. Lin, B. S. Y. Ung, J. Balakrishnan, B. W.-H. Ng, B. Ferguson, S. P. Mickan, B. M. Fischer, and D. Abbott, "T-ray sensing and imaging," *Proc. IEEE* , vol. 95, no. 8, pp. 1528–1558, Aug. 2007.

[12] H.-B. Liu, H. Zhong, N. Karpowicz, Y. Chen, and X.-C. Zhang, "Terahertz spectroscopy and imaging for defense and security applications," *Proc. IEEE*, vol. 95, no. 8, pp. 1514–1527, Aug. 2007.

[13] R. Arusi, Y. Pinhasi, B. Kapilevitch, D. Hardon, B. Litvak, and M. Anisimov, "Linear FM radar operating in the Tera-Hertz regime for concealed objects detection," in *Proc. Int. Conf. Microw., Commun., Antennas Electron. Syst.*, 2009, pp. 1–4.

[14] E. Öjefors, U. R. Pfeiffer, A. Lisauskas, and H. G. Roskos, "A 0.65 THz focal-plane array in a quarter-micron CMOS process technology," *IEEE J. Solid-State Circuits*, vol. 44, no. 7, pp. 1968–1976, Jul. 2009.

[15] K. B. Cooper, R. J. Dengler, N. Llombart, T. Bryllert, G. Chattopadhyay, I. Mehdi, and P. H. Siegel, "An approach for sub-second imaging of concealed objects using terahertz (THz) radar," *J. Infrared, Millim. Terahertz Waves*, vol. 30, no. 12, pp. 1297–1307, 2009.

[16] R. Appleby and H. B. Wallace, "Standoff detection of weapons and contraband in the 100 GHz to 1 THz region," *IEEE Trans. Antenna Propag.*, vol. 55, no. 11, pp. 2944–2956, Nov. 2007.

[17] M. J. Rosker and H. B. Wallace, "Imaging through the atmosphere at terahertz frequencies," in *IEEE MTT-S Int. Microw. Symp. Dig.*, 2007, pp. 773–776.

[18] R. J. Dengler, K. B. Cooper, G. Chattopadhyay, I. Mehdi, E. Schlecht, A. Skalare, C. Chen, and P. H. Siegel, "600 GHz imaging radar with 2 cm range resolution," in *IEEE MTT-S Int. Microw. Symp. Dig.*, 2007, pp. 1371–1374.

[19] J. F. Federici, D. Gary, R. Barat, and Z.-H. Michalopoulou, "T-rays versus terrorists, terahertz radiation lets security screeners find bombs and weapons wherever they're hidden," *IEEE Spectr.*, vol. 44, no. 7, pp. 47–52, Jul. 2007.

[20] J. F. Federici, B. Schulkin, F. Huang, D. Gary, R. Barat, F. Oliveira, and D. Zimdars, "THz imaging and sensing for security applications – Explosives, weapons and drugs," *Semicond. Sci. Technol.*, vol. 20, pp. S266–S280, 2005.

[21] J. Grade, P. Haydon, and D. van der Weide, "Electronic terahertz antennas and probes for spectroscopic detection and diagnostics," *Proc. IEEE*, vol. 95, no. 8, pp. 1583–1591, Aug. 2007.

[22] D. R. Vizard and R. Doyle, "Invited paper : Advances in millimeter wave imaging and radar systems for civil applications," in *IEEE MTT-S Int. Microw. Symp. Dig.*, 2006, pp. 94–97.

[23] R. Appleby, "The potential for stand-off detection of ieds between 100 GHz and 1 THz," in *IEEE MTT-S Int. Microw. Symp. Dig.*, 2007, pp. 70–78.

[24] D. Matheson, "Trends in the development of THz receiver technology," in *IEEE MTT-S Int. Microw. Symp. Dig.*, 2007, pp. 30–39.

[25] Z. Zhang and T. Buma, "Terahertz impulse imaging with sparse arrays and adaptive reconstruction," *IEEE J. Sel. Topics Quantum Electron.*, to be published.

[26] D. O. Komeev, L. Y. Bogdanov, and A. V. Nalivkin, "Passive millimeter wave imaging system with white noise illumination for concealed weapons detection," in *Proc. Joint 29th Int. Conf. Infrared Millim. Waves 12th Int. Conf. Terahertz Electron.*, Karlsruhe, Germany, 2004, pp. P2.72–P2.73.

[27] T. D. Dorney, W. W. Symes, R. G. Baraniuk, and D. M. Mittleman, "Terahertz multi-static reflection imaging," *J. Opt. Soc. Amer. A, Opt. Image Sci.*, vol. 19, no. 7, pp. 1432–1442, Jul. 2002.

[28] H. Banks, "Electromagnetic interrogation and detection problems in dielectric materials," NC State Univ., Raleigh, Mar. 22, 2004.

[29] T. Dogaru, L. Collins, and L. Carin, "Optimal time-domain detection of a deterministic target buried under a randomly rough interface," *IEEE Trans. Antennas Propag.*, vol. 49, no. 3, pp. 313–326, Mar. 2001.

[30] "Inspec alerts, image sensors," IEE Inspec current awareness," INSPEC, Stevenage, U.K., Tech. Rep. Issue 2003-002, 2003.

[31] E. Donahue, "Terahertz technology and hyperspectral imaging: Cutting-edge approaches to Homeland Security and medical imaging," Northeastern Univ., Boston, MA, 2003. [Online]. Available: http://www.nupr.neu.edu/11-03/censsis.html

[32] T.-K. Chan, Y. Kuga, and A. Ishimaru, "Subsurface detection of a buried object using angular correlation function measurement," *Waves in Random Media*, vol. 7, pp. 457–465, 1997.

[33] D. D. Eden, "Antenna-coupled microbolometer millimeter wave focal plane array technology," *Proc. SPIE—Int. Soc. Opt. Eng.*, vol. 4719, pp. 370–381, 2002.

[34] Luukanen, A. J. Miller, and E. N. Grossman, "Active millimeter-wave video rate imaging with a staring 120-element microbolometer array," *Proc. SPIE—Int. Soc. Opt. Eng.*, vol. 5410, Radar Sensor Technol. VIII and Passive Millim.-Wave Imaging Technol. VII, pp. 195–201, 2004.

[35] R. Doyle, B. Lyons, J. Walshe, P. Curtin, A. H. Lettington, T. McEnroe, and J. McNaboe, "Low cost millimeter wave camera imaging up to 140 GHz," in *Proc. 34th Eur. Microw. Conf.*, 2004, pp. 1285–1288.

[36] R. Appleby, "Passive millimeter-wave imaging and how it differs from terahertz imaging," *Phil. Trans. Roy. Soc. London A, Math. Phys. Sci.*, vol. 362, pp. 379–394, 2004.

[37] A. H. Lettington, D. Dunn, M. Attia, and I. M. Blankson, "Passive millimeter-wave imaging architectures," *J. Opt. A, Pure Appl. Opt.*, vol. 5, no. 4, p. S103.

[38] J. W. Archer and M. G. Shen, "176–200 GHz receiver module using indium phosphide and gallium arsenide MMICs," *Microw. Opt. Technol. Lett.*, vol. 43, pp. 458–462, 2004.

[39] J. W. Archer and M. G. Shen, "W-band transmitter module using gallium arsenide MMICs," *Microw. Opt. Technol. Lett.*, vol. 42, pp. 210–213, 2004.

[40] R. Doyle, B. Lyons, A. Lettington, T. McEnroe, J. Walshe, J. McNaboe, P. Curtin, and S. Bleszynski, "Stand-off detection of hidden threat objects on personnel at checkpoints and in public areas using active millimeter-wave imaging," *Proc. SPIE—Int. Soc. Opt. Eng.*, vol. 5619, Passive Millim.-Wave Terahertz Imaging Technol., pp. 90–97, 2004.

[41] D. Macfarlane, J. Lesurf, and D. Robertson, "Close-range millimeter wave imaging," *Proc. SPIE—Int. Soc. Opt. Eng.*, vol. 4719, pp. 350–358, 2002.

[42] P. F. Goldsmith, C.-T. Hsieh, G. R. Huguenin, J. Kapitzky, and E. L. Moore, "Focal plane imaging systems for millimeter wavelengths," *IEEE Trans. Microw. Theory Tech.*, vol. 41, no. 10, pp. 1664–1675, Oct. 1993.

[43] C. Martin, S. Clark, J. Lovberg, and J. Galliano, "Real-time wide field of view passive millimeter-wave imaging," *Proc. SPIE—Int. Soc. Opt. Eng.*, vol. 4719, pp. 341–349, 2002.

[44] Y. A. Pirogov, V. V. Gladun, S. P. Chzhen, D. A. Tischenko, and A. L. Timanovskiy, "Radio thermal images of natural objects in 8-mm and 3-mm ranges," *Proc. SPIE—Int. Soc. Opt. Eng.*, vol. 4719, pp. 318–326, 2002.

[45] J. Richter, D. Notel, F. Kloppel, J. Huck, H. Essen, and L.-P. Schmidt, "A multi-channel radiometer with focal plane array antenna for W-band passive millimeter-wave imaging," in *IEEE MTT-S Int. Microw. Symp. Dig.*, 2006, pp. 1592–1595.

[46] R. Appleby, G. Holst, and D. Wikner, Eds., "Infrared and passive millimeter-wave imaging systems: Design, analysis, modeling, and testing," in *Proc. SPIE—Int. Soc. Opt. Eng.*, 2002, vol. 4719, pp. 1–420.

[47] P. Moffa, L. Yujiri, H. Agravante, G. De Amici, D. Dixon, S. Fornaca, C. Jackson, T. Jaeger, K. Jordan, R. Quon, K. Rasmussen, T. Samec, and M. Shoucri, "Large-aperture passive millimeter-wave push broom camera," in *Proc. SPIE–Int. Soc. Opt. Eng.*, 2001, vol. 4373, pp. 1–6.

[48] S. Weinreb, R. Lai, N. Erickson, T. Gaier, and J. Wielgus, "W-band InP wideband MMIC LNA with 30 K noise temperature," in *IEEE MTT-S Int. Microw. Symp. Dig.*, 1999, pp. 101–104.

[49] J. W. May and G. M. Rebeiz, "Design and characterization of W-band SiGe RFICs for passive millimeter-wave Imaging," *IEEE Trans. Microw. Theory Tech.*, vol. 58, no. 2, pp. 1420–1430, Feb. 2010.

[50] P. Kangaslahti, T. Gaier, D. Dawson, J. Tuovinen, T. Kartaavi, M. Lahdes, N. J. Hughes, T. L. Cong, P. Jukkala, P. Sjöman, and S. Weinreb, "Low-noise amplifiers in InP technology for pseudo correlating millimeter wave radiometer," in *IEE MTT-S Int. Microw. Symp. Dig.*, 2001, pp. 1959–1962.

[51] N. Gopalsami and A. Raptis, "Millimeter-wave imaging of thermal and chemical signatures," in *Proc. SPIE–Int. Soc. Opt. Eng.*, 1999, vol. 3703, pp. 130–138.

[52] C.-C. Wang, S. Trivedi, F. Jin, J. Khurgin, D. Temple, U. Hommerid, E. Gad, and A. Corder, "Interferometer-less coherent optical range finder," in *CLEO Tech. Dig.*, 2001, pp. 376–377.

[53] G. Sinclair, P. Coward, R. N. Anderton, R. Appleby, T. Seys, and P. Southwood, "Detection of illegal passengers in lorries using a passive millimeter wave scanner," in *Proc. 36th Annu. Int. Carnahan Conf. Security Technol.*, 2002, pp. 167–170.

[54] G. Sinclair, R. Appleby, P. Coward, and S. Price, "Passive millimeter-wave imaging in security scanning," in *Proc. SPIE–Int. Soc. Opt. Eng.*, 2000, vol. 4032, pp. 40–45.

[55] S. Price, R. N. Anderton, J. R. Borrill, P. R. Coward, M. J. Roberts, N. A. Salmon, G. N. Sinclair, M. R. M. Wasley, K. S.-J. Murphy, R. Appleby, A. H. Lettington, D. Dunn, P. Papakosta, and I. Thomas, "Compact video-rate passive millimeter-wave imager," in *Proc. Int. Conf. Infrared Millim. Waves*, Colchester, U.K., 1998, pp. 13–19.

[56] D. G. Macfarlane, J. C. G. Lesurf, and D. A. Robertson, "Close range millimeter wave imaging," *Proc. SPIE—Int. Soc. Opt. Eng.*, vol. 4719, pp. 350–358, 2002.

[57] Pergande, L. Mirth, L. Anderson, and P. Benson, "Commercialisation aspects of a MMW camera," *Proc. SPIE—Int. Soc. Opt. Eng.*, vol. 4719, pp. 359–363, 2002.

[58] E. N. Grossman, A. K. Bhupathiraju, A. J. Miller, and C. D. Reintsema, "Concealed weapons detection using an uncooled millimeter-wave microbolometer system," *Proc. SPIE—Int. Soc. Opt. Eng.*, vol. 4719, pp. 364–369, 2002.

[59] T. Lüthi and C. Mätzler, "Stereoscopic passive millimeter-wave imaging and ranging," *IEEE Trans. Microw. Theory Tech.*, vol. 53, no. 8, pp. 2594–2599, Aug. 2005.

[60] A. Lisauskas, U. Pfeiffer, E. Ojefors, P. H. Bolivar, D. Glaab, and H. G. Roskos, "Rational design of high-responsivity detectors of terahertz radiation based on distributed self-mixing in silicon field-effect transistors," *J. Appl. Phys.*, vol. 105, no. 11, pp. 114511–114518, 2009.

[61] E. Öjefors and U. R. Pfeiffer, "A 650 GHz SiGe receiver front-end for terahertz imaging arrays," in *ISSCC Conf. Dig.*, 2010, pp. 430–431.

[62] L. V. Volkov, A. I. Voronko, N. L. Volkova, and A. R. Karapetyan, "Active MMW imaging technique for contraband detection," in *Proc. 33th Eur. Microw. Conf.*, 2003, pp. 531–534.

[63] K. Watabe, K. Shimizu, M. Yoneyama, and K. Mizuno, "Millimeter-wave active imaging using neural networks for signal processing," *IEEE Trans. Microw. Theory Tech.*, vol. 51, no. 5, pp. 1512–1516, May 2003.

[64] K. Mizuno, "Millimeter wave imaging technologies," in *Proc. APMC*, Taipei, Taiwan, 2001, pp. 1–2.

[65] V. I. Fedorov, S. S. Popova, and A. N. Pisarchik, "Dynamic effects of submillimeter wave radiation on biological objects of various levels of organization," *Int. J. Infrared Millim. Waves*, vol. 24, no. 8, pp. 1235–1254, 2003.

[66] Pakhomov, H. Prol, and Y. Kyel, "A pilot study of the millimeter-wavelength radiation effect on synaptic transmission," *Electro-Magnetobiol.*, vol. 17, no. 2, pp. 115–25, 1998.

[67] M. Swicord and Q. Balzano, "Has electromagnetic energy in the band 0.1–100 GHz useful medical applications? A review of mechanisms and biological database offers dim prospects," *IEEE Trans. Plasma Sci.*, vol. 36, no. 4, pp. 1638–1649, Aug. 2008.

[68] D. M. Sheen, D. L. McMakin, and T. E. Hall, "Cylindrical millimeter-wave imaging technique and applications," *Proc. SPIE—Int. Soc. Opt. Eng.*, vol. 6211, Passive Millim.-Wave Imaging Technol. IX, pp. 6357–6365, 2006.

[69] D. W. Van Der Weide, J. Murakowski, and F. Keilmann, "Spectroscopy with electronic terahertz techniques," *Proc. SPIE—Int. Soc. Opt. Eng.*, vol. 3828, Terahertz Spectroscopy Applic. II, pp. 276–284, 1999.

[70] D. W. Van der Weide, J. Murakowski, and F. Keilmann, "Gas-absorption spectroscopy with electronic terahertz techniques," *IEEE Trans. Microw. Theory Tech.*, vol. 48, no. 4, pp. 740–743, Apr. 2000.

[71] S. Vainshtein, J. Kostamovaara, Y. Sveshnikov, S. Gurevich, M. Kulagina, V. Yuferev, L. Shestak, and M. Sverdlov, "Superfast high-current switching of GaAs avalanche transistor," *Electron. Lett.*, vol. 40, no. 1, pp. 1–2, 2004.

[72] M. Fortin, M. Piché, and E. F. Borra, "Optical tests with Bessel beam interferometry," *Opt. Exp.*, vol. 12, no. 24, pp. 5887–5895, 2004.

[73] V. S. Ilchenko, M. Mohageg, A. A. Savchenkov, A. B. Matsko, and L. Maleki, "Efficient generation of truncated Bessel beams using cylindrical waveguides," *Opt. Exp.*, vol. 15, no. 9, p. 5866, 2007.

[74] J. L. Bauck and W. K. Jenkins, "Tomographic processing of spotlight-mode synthetic aperture radar signals with compensation for wavefront curvature," in *Proc. ICASSP*, 1988, pp. 1192–1195.

[75] R. C. Hansen, *Microwave Scanning Antennas*. New York: Academic, 1966, vol. I, Array Systems.

[76] B. Shen and W. L. Stutzman, "A scanning spherical tri-reflector antenna with a moving flat mirror," *IEEE Trans. Antennas Propag.*, vol. 43, no. 3, pp. 270–276, Mar. 1995.

[77] N. A. Agapov, "Two-mirror scanning system," *Sov. J. Opt. Technol.*, vol. 53, no. 6, pp. 324–325, 1986.

[78] V. G. Borkar, B. K. Mukhopadhyay, J. V. Prasad, V. M. Pandharipande, and R. Ethiraj, "A millimeter-wave monopulse twist reflector scanning antenna system: Theory and experiment," *IETE J. Res.*, vol. 43, no. 6, pp. 415–421, 1997.

[79] S. Campana, *Passive Electro-Optical Systems, The Infrared and Electro-Optical Systems Handbook*. Bellingham, WA: SPIE, 1993, vol. 5.

[80] X. Feng, J. R. Schott, and T. W. Gallagher, "Modelling the performance of a high-speed scan mirror for an airborne line scanner," *Opt. Eng.*, vol. 33, no. 4, pp. 1214–1222, 1994.

[81] R. Appleby, S. Price, and A. H. Lettington, "Passive millimeter wave imaging—Seeing through cloud and fog," in *Proc. Roy. Aeronaut. Soc.*, 1994, pp. 2.1–2.7.

[82] A. H. Lettington, "GB Pat. Specification ," U.K. 981906408.

[83] P. Corredoura, Z. Baharav, B. Taber, and G. Lee, "Millimeter-wave imaging system for personnel screening: Scanning 10^7 points a second and using no moving parts," *Proc. SPIE—Int. Soc. Opt. Eng.*, vol. 6211, pp. 62110B.1–62110B.8, 2006.

[84] M. K. Choi, A. D. Bettermann, and D. W. Van der Weide, "Biological and chemical sensing with electronic THz techniques," *Proc. SPIE—Int. Soc. Opt. Eng.*, vol. 5268, Chem. Biolog. Standoff Detection, pp. 27–35.

[85] W. L. Chan *et al.*, "Imaging with terahertz radiation," *Rep. Prog. Phys.*, vol. 70, pp. 1325–137, 2007.

[86] T. Löffler, K. J. Siebert, N. Hasegawa, T. Hahn, and H. G. Roskos, "All-optoelectronic terahertz imaging systems and examples of their application," *Proc. IEEE*, vol. 95, no. 8, pp. 1576–1582, Aug. 2007.

[87] Y.-C. Shen and P. F. Taday, "Development and application of terahertz pulsed imaging for nondestructive inspection of pharmaceutical tablet," *IEEE J. Sel. Topics Quantum Electron.*, vol. 14, no. 2, pp. 407–415, Mar./Apr. 2008.

[88] D. Saeedkia and S. Safavi-Naeini, "Terahertz photonics: Optoelectronic techniques for generation and detection of terahertz waves," *J. Lightw. Technol.*, vol. 26, no. 15, pp. 2409–2423, Aug. 2008.

[89] D. A. Zimdars, "Fiber-pigtailed terahertz time domain spectroscopy instrumentation for package inspection and security imaging," *Proc. SPIE—Int. Soc. Opt. Eng.*, vol. 5070, pp. 108–116, 2003.

[90] D. Zimdars and J. S. White, "Terahertz reflection imaging for package and personnel inspection," *Proc. SPIE—Int. Soc. Opt. Eng.*, vol. 5411, pp. 78–83, 2004.

[91] B. Sartorius, H. Roehle, H. Künzel, J. Böttcher, M. Schlak, D. Stanze, H. Venghaus, and M. Schell, "All-fiber terahertz time-domain spectrometer operating at 1.5 μm telecom wavelengths," *Opt. Exp.*, vol. 16, pp. 9565–9570, 2008.

[92] N. Vieweg, N. Krumbholz, T. Hasek, R. Wilk, V. Bartels, C. Keseberg, V. Pethukhov, M. Mikulics, L. Wetenkamp, and M. Koch, "Fiber-coupled THz spectroscopy for monitoring polymeric compounding processes," *Polymer Testing*, vol. 28, no. 1, pp. 30–35, 2009.

[93] B. Ferguson, S. Wang, D. Gray, D. Abbott, and X.-C. Zhang, "T-ray computed tomography," *Opt. Lett.*, vol. 27, pp. 1312–1314, 2002.

[94] J. Pearce, H. Choi, D. M. Mittleman, J. White, and D. Zimdars, "Terahertz wide aperture reflection tomography," *Opt. Lett.*, vol. 30, pp. 1653–1655, 2005.

[95] X. Shen, C. R. Dietlein, E. Grossman, Z. Popovic, and F. G. Meyer, "Detection and segmentation of concealed objects in terahertz images," *IEEE Trans. Image Process.*, vol. 17, no. 12, pp. 2465–2475, Dec. 2008.

[96] H. D. Griffiths and C. J. Baker, "Radar imaging for combatting terrorism,," in *Imaging for Detection and Identification*, J. Byrnes, Ed. Berlin, Germany: Springer, 2007.

[97] R. Bamler, "A comparison of range-Doppler and wavenumber domain SAR focusing al-gorithms," *IEEE Trans. Geosci. Remote Sens.*, vol. 30, no. 4, pp. 706–713, Jul. 1992.

[98] W. G. Carrara, R. S. Goodman, and R. M. Majewski, *Spotlight Synthetic Aperture Radar: Signal Processing Algorithms*. Norwood, MA: Artech House, 1995.

[99] D. A. Ausherman, A. Kozma, J. L. Walker, H. M. Jones, and E. C. Poggio, "Developments in radar imaging," *IEEE Trans. Aerosp. Electron. Syst.*, vol. AES-20, no. 4, pp. 363–400, Jul. 1984.

[100] Averbuch, R. R. Coifman, D. L. Donoho, M. Elad, and M. Israeli, "Fast and accurate polar Fourier transform," *Appl. Comput. Harmon. Anal.*, vol. 21, pp. 145–167, 2006.

[101] Averbuch, R. R. Coifman, D. L. Donoho, M. Israeli, and J. Waldén, "Fast slant stack: A notion of radon transform for data in a Cartesian grid which is rapidly computable, algebraically exact, geometrically faithful and invertible," *Appl. Comput. Harmon.*, vol. 21, pp. 145–167, 2006.

[102] S. R. J. Axelsson, "Beam characteristics of three-dimensional SAR in curved or random paths," *IEEE Trans. Geosci. Remote Sens.*, vol. 42, no. 10, pp. 2324–2334, Oct. 2004.

[103] N. J. Redding and T. M. Payne, "Inverting the spherical Radon transform for 3-D SAR image formation," in *Proc. Int. Conf. Radar*, 2003, pp. 466–471.

[104] N. J. Redding, "SAR image formation via inversion of Radon transforms," in *Proc. IEEE ICIP*, 2004, pp. 13–16.

[105] J. D. Coker and A. H. Tewfik, "Multistatic SAR image reconstruction based on an elliptical-geometry Radon transform," in *Proc. Int. Waveform Diversity Design Conf.*, Jun. 2007, pp. 204–208.

[106] J. D. Coker and A. H. Tewfik, "Random sampling strategies in multistatic SAR," in *Proc. IEEE ICASSP*, 2008, pp. 2461–2464.

[107] S. Kidera, Y. Kani, T. Sakamoto, and T. Sato, "An experimental study for a high-resolution 3-D imaging algorithm with linear array for UWB radars," in *Proc. IEEE Int. Conf. Ultra-Wideband*, 2007, pp. 1–6.

[108] T. Sakamoto and T. Sato, "Real-time imaging of human bodies with UWB radars using walking motion," in *Proc. IEEE Int. Conf. Ultra-Wideband*, 2007, pp. 26–30.

[109] A. F. Yegulalp, "Fast backprojection algoritm for synthetic aperture radar," in *Proc. IEEE Radar Conf.*, 1999, pp. 60–65.

[110] S. Basu and Y. Bresler, "$\mathrm{O}(\mathrm{N3}\log \mathrm{N})$ backprojection algorithm for Radon transform," *IEEE Trans. Med. Imag.*, vol. 21, pp. 76–88, Feb. 2002.

[111] L. M. H. Ulander, H. Hellsten, and G. Stenström, "Synthetic-aperture radar processing using fast factorized back-projection," *IEEE Trans. Aerosp. Electron. Syst.*, vol. 39, no. 3, pp. 76–88, Feb. 2003.

[112] S. Xiao, D. C. Munson Jr., S. Basu, and Y. Breslert, "An $\mathrm{N2}\log \mathrm{N}$ back-projection algorithm for SAR image formation," in *Conf. Rec. 34th Asilomar Conf. Signals, Syst., Comput.*, 2000, pp. 3–7.

[113] Y. Ding and D. C. Munson Jr., "A fast back-projection algorithm for bistatic SAR imaging," in *Proc. ICIP*, 2002, vol. 2, pp. 449–452.

[114] F. Rocca, C. Cafforio, and C. Prati, "Synthetic aperture radar: A new application for wave equation techniques," *Geophys. Prospecting*, vol. 37, pp. 809–830, 1989.

[115] Cafforio, C. Prati, and F. Rocca, "SAR data focusing using seismic migration techniques," *IEEE Trans. Aerosp. Electron. Syst.*, vol. 27, no. 2, pp. 194–206, Mar. 1991.

[116] Cafforio, C. Prati, and F. Rocca, "Full resolution focusing of SEASAT SAR images in the frequency-wave number domain," in *Proc. 8th EARSelL Symp.*, Capri, Italy, 1988, pp. 336–355.

[117] R. K. Raney, H. Runge, R. Bamler, I. G. Cumming, and F. H. Wong, "Precision SAR proc-essing using chirp scaling," *IEEE Trans. Geosci. Remote Sens.*, vol. 32, no. 4, pp. 786–799, Jul. 1994.

[118] Subiza, E. GienoNieves, J. M. Lopez-Sanchez, and J. Fortuny-Guasch, "Non-uniform FFT's (NUFFT) algorithms applied to SAR imaging," *Proc. SPIE—Int. Soc. Opt. Eng.*, vol. 5236, pp. 72–79, 2004.

[119] Y. Zhang-O'Connor and J. A. Fessler, "Fourier-based forward and back-projectors in iterative fan-beam tomographic image reconstruction," *IEEE Trans. Med. Imaging*, vol. 25, no. 5, pp. 582–589, May 2006.

[120] S. S. Ahmed, A. Schiessl, and L.-P. Schmidt, "Near field mm-wave imaging with multistatic sparse 2D-arrays," in *Proc. 6th Eur. Radar Conf.*, Oct. 2009, pp. 180–183.

[121] Y. Na, H. Sun, Y. H. Lee, L. C. Tai, and H. L. Chan, "Performance evaluation of back-projection and range migration algorithms in foliage penetration radar imaging," in *Proc. IEEE ICIP*, 2004, pp. 21–24.

[122] A. R. Thompson, J. M. Moran, and G. W. Swenson, *Interferometry and Synthesis in Radio Astronomy*. Melbourne, FL: Krieger, 1991.

[123] N. Skou and D. Le Vine, *Microwave Radiometer Systems; Design And Analysis*. Norwood, MA: Artech House, 2006.

[124] C. S. Ruf, "Numerical annealing of low-redundancy linear arrays," *IEEE Trans. Antenna Propag.*, vol. 41, no. 1, pp. 85–90, Jan. 1993.

[125] K. P. Walsh, B. Schulkin, D. Gary, J. F. Federici, R. Barat, and D. Zimdars, "Terahertz near-field interferometric and synthetic aperture imaging," *Proc. SPIE—Int. Soc. Opt. Eng.*, vol. 5411, Terahertz for Military Security Applic. II, pp. 5411–5419, 2004.

[126] J. O'Hara and D. Grischkowsky, "Synthetic phase-array terahertz imaging systems," *Opt. Lett.*, vol. 27, no. 12, pp. 1070–1072, 2002.

[127] J. O'Hara and D. Grischkowsky, "Quasi-optic synthetic phased-array terahertz imaging," *J. Opt. Soc. Amer. B, Opt. Phys.*, vol. 21, no. 6, pp. 1178–1191, Jun. 2004.

[128] G. Arnold, P. Chen, A. Heryudono, J. Nam, J. M. Ramirez, and N. Williams, "Sparse aperture radar imaging," Mathematical Modeling in Industry IX, Univ. of Minnesota, Minneapolis, Tech. Rep., 2005.
[129] M. Bertero and P. Boccacci, *Introduction to Inverse Problems in Imaging*. Bristol, U.K.: Inst. Phys., 1998.
[130] A. N. Tikhonov and V. Y. Arsenine, *Solution of Ill Posed Problem*. Washington, DC: Wiston-Wiley, 1977.
[131] H. T. Banks, N. L. Gibson, and W. P. Winfree, "Electromagnetic crack detection inverse problems using terahertz interrogating signals," NASA, Center Res. Sci. Computation, North Carolina State Univ., Raleigh, NC, 2003.
[132] B. Sartorius *et al.*, "All-fiber terahertz time-domain spectrometer operating at 1.5 μm wavelengths," *Opt. Exp.*, vol. 16, pp. 9565–9570, 2008.
[133] P. R. Smith, D. H. Auston, and M. C. Nuss, "Subpicosecond photoconducting dipole antennas," *IEEE J. Quantum Electron.*, vol. 24, no. 2, pp. 255–260, Feb. 1988.
[134] K. W. DeLong, R. Trebino, J. Hunter, and W. E. White, "Frequency-resolved optical gating with the use of second-harmonic generation," *J. Opt. Soc. Amer. B, Opt. Phys.*, vol. 11, pp. 2206–2215, 1994.
[135] G. P. Agrawal, *Nonlinear Fiber Optics*, 4th ed. New York: Academic, 2006.

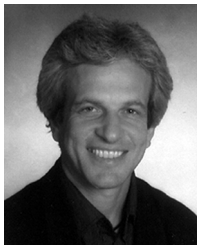

Viktor Krozer (M'91–SM'03) received the Dipl.-Ing. and Dr.-Ing. degrees in electrical engineering from the Technical University of Darmstadt (TU Darmstadt), Darmstadt, Germany, in 1984 and 1991, respectively.

In 1991, he became a Senior Scientist with TU Darmstadt, where he was involved with high-temperature microwave devices and circuits and submillimeter-wave electronics. From 1996 to 2002. he was a Professor with the Technical University of Chemnitz, Chemnitz, Germany. From 2002 to 2009, he was a Professor with Electromagnetic Systems, DTU Elektro, Technical University of Denmark, Copenhagen, Denmark, and was Head of the Microwave Technology Group. Since 2009, he has been the endowed Oerlikon-Leibniz-Goethe Professor for Terahertz Photonics at the Johann Wolfgang Goethe University Frankfurt, Frankfurt, Germany. His research areas include terahertz electronics, monolithic microwave integrated circuits, nonlinear circuit analysis and design, device modeling, and remote sensing instrumentation.

Torsten Löffler was born in Winterberg, Germany, in 1970. He received the Diploma in physics from RWTH Aachen, Aachen, Germany, and the Ph.D. degree from the Johann Wolfgang Goethe University Frankfurt, Frankfurt, Germany, in 2003.

Based on his continued research, he founded the Loeffler Technology GmbH (LTG) in 2007 to commercialize terahertz technology and to develop the first products. In January 2009, LTG became SynView GmbH, Frankfurt, Germany, to enter the industrial nondestructive testing market. He holds several patents and has authored or coauthored more than 50 publications, most of them on terahertz technology. At SynView GmbH, he is focusing on the technology and product development as well as the technical evaluation of potential applications. In addition, he serves the scientific customers and leads all public funded projects.

Jørgen Dall (M'07) received the M.Sc. degree in electrical engineering and Ph.D. degree from the Technical University of Denmark, Kongens Lyngby, Denmark, in 1984 and 1989, respectively.

In the 1990s, he worked with the Danish airborne SAR system, EMISAR. He led the development of dedicated onboard and offline processors, and he was responsible for the EMISAR data processing. From 1996 to 2001, he also organized the EMISAR data acquisition campaigns and served as Mission Manager. Since 1993, he has been an Associate Professor with the Technical University of Denmark, Copenhagen, Denmark. Currently, he is leading the development of an airborne polarimetric ice sounding radar for the European Space Agency. His research includes design of advanced radar altimeters for planetary missions, development of SAR signal processing techniques, polarimetric SAR interferometry, polarimetric and interferometric SAR calibrations, and SAR applications within ice mapping, etc.

Anders Kusk (M'02) received the M.Sc. and Ph.D. degrees in electrical engineering from the Technical University of Denmark, Copenhagen, Denmark, in 2002 and 2006, respectively.

Since 2006, he has been with the Microwaves and Remote Sensing Group at DTU Space, Technical University of Denmark, working with radar signal processing, SAR imaging, and remote sensing instrumentation.

Finn Eichhorn received the B.Sc. degree in electrical engineering from Odense University, Odense, Denmark, in 2004, M.Sc. degree in electronics engineering and Ph.D. degree from the Technical University of Denmark (DTU), Copenhagen, Denmark, in 2006, and 2009, respectively.

Since 2009, he has been a Postdoctoral Researcher with DTU. His research interests include terahertz science and technology and the application of fiber technology in terahertz systems. He is especially interested in technical 2-D and 3-D imaging with terahertz radiation and various radiation and scattering phenomena of terahertz waves.

Rasmus Kjelsmark Olsson received the M.Sc. degree in physics from the University of Copenhagen, Copenhagen, Denmark, in 2006, and is currently working toward the Ph.D. degree at the Technical University of Denmark.

Jonas Due Buron received the M.Eng. degree in physics and nanotechnology from the Technical University of Denmark (DTU), Copenhagen, Denmark, in 2010.

He is currently a Research Assistant with the Terahertz Technologies and Biophotonics Group, DTU. His areas of research include ultrafast carrier dynamics in graphene, terahertz time-domain spectroscopy, and terahertz near-field microscopy.

Peter Uhd Jepsen received the M.Sc. degree in physics and chemistry from Odense University, Odense, Denmark, in 1994, and the Ph.D. degree in natural sciences from Århus University, Århus, Denmark, in 1996.

He was with the University of Freiburg, Freiburg, Germany, from 1996 to 2004, working with terahertz time-domain spectroscopy. In 2005, he became an Associate Professor with the Technical University of Denmark (DTU), Copenhagen, Denmark, and, since 2008, he has been a Full Professor and Head of the

Terahertz Technologies and Biophotonics Group, DTU. His research areas include photonics-based terahertz technology, broadband spectroscopy, ultrafast lasers, and time-resolved terahertz spectroscopy.

Vitaliy Zhurbenko (S'04–M'09) received the B.Sc. and M.Sc. degrees from the Kharkiv National University of Radio Electronics, Kharkiv, Ukraine, in 2000 and 2001, respectively, and the Ph.D. degree from the Technical University of Denmark, Copenhagen, Denmark, in 2008, all in electrical engineering.

From November 2000 to June 2005, he was a Metrology Engineer with the Laboratory of Metrology, Kharkiv, Ukraine. In 2004, he became a Junior Member of the Teaching Staff with the Kharkiv National University of Radio Electronics. In 2005, he joined the Technical University of Denmark, where he is currently a Postdoctoral Researcher. His current teaching and research interests include microwave and millimeter-wave sensing for biomedical and security applications, microwave imaging and radar systems as well as related algorithms and data processing, microwave and millimeter-wave devices and integrated circuits for instrumentation applications, antenna and passive circuit design and characterization, and electromagnetic metamaterials.

Thomas Jensen received the M.Sc. degree from the Technical University of Denmark (DTU), Copenhagen, Denmark, in 2005, and is currently working toward the Ph.D. degree at DTU Elektro, DTU, focusing on packaging of radar circuits utilizing LTCC microwave multilayer technology.

As a Research Assistant with Electromagnetic Systems, DTU Elektro, DTU, he has been involved with radiometer instrument design and terahertz imaging systems.